View metadata, citation and similar papers at core.ac.uk
brought to you by CORE
provided by Digital.CSIC

Thermal instability of implanted Mn ions in ZnO

J. A. Sans,[1,a] G. Martínez-Criado,[1] J. Susini,[1] R. Sanz,[2] J. Jensen,[3] I. Minguez,[2] M. Hernandez-Velez,[4] A. Labrador,[5] and P. Carpentier[6]
[1]*European Synchrotron Radiation Facility (ESRF), F-38043 Grenoble, France*
[2]*Instituto de Ciencia de Materiales de Madrid (CSIC), Carretera de Colmenar Viejo, Cantoblanco, 28049 Madrid, Spain*
[3]*Thin Film Physics, Department of Physics, Chemistry and Biology, Linköping University, SE-581 83 Linköping, Sweden*
[4]*Departamento de Fisica Aplicada, Facultad de Ciencias, Campus Universitario de Cantoblanco, 28049 Madrid, Spain*
[5]*BM16-CRG, Consorci Laboratori de Llum de Sincrotró (LLS), c/o ESRF, F-38043 Grenoble, France*
[6]*Institut de Biologie Structurale, CNRS/CEA/UJF, F-38027 Grenoble, France*

(Received 30 June 2009; accepted 24 November 2009; published online 25 January 2010)

This letter reports on the site configuration of implanted Mn cations in ZnO. The samples studied were obtained by means of ion implantation in m-plane ZnO single crystals. Synchrotron radiation based fluorescence shows no contamination during the implantation process. The results of micro-x-ray absorption spectroscopy indicate that Mn ions are located in substitutional sites without detectable traces of secondary phases. The postgrowth thermal annealing in O_2 atmosphere induces a change in the coordination of a large amount of Mn cations, corresponding to α-Mn_2O_3. © *2010 American Institute of Physics*. [doi:10.1063/1.3275890]

I. INTRODUCTION

The study of alloys of ZnO with transition metals (TMs) have attracted a lot of interest in the past years due to its possible application in spintronic devices. The explanation of the origin of the magnetic properties, concretely ferromagnetism, in these wide band-gap materials has triggered the publication of a lot of papers with controversial results. These articles can be split into two categories depending on the local structure of TM in the wide band-gap material. On the one hand, considering the substitutional site of TM into the host lattice,[1] several explanations had been proposed such as a hole mediated exchange Zener model published by Dietl *et al.*[2] or due to exchange mediated by carriers in a spin-split-orbit impurity band derived from extended orbitals in donor centers.[3] On the other hand, the possible ferromagnetism is considered to come from clusters[4] or segregation of different TM oxides.[5–7]

One of the most important factors in order to obtain reliable results is the growth method. In this framework, the ion implantation has shown several advantages[8] with respect to other growth techniques, such as the control of the ion fluency and the use of an isotopically pure ionic beam, but also some disadvantages[9] such as the damage produced on surface. Fortunately, the application of thermal annealing in oxidizing conditions reduces the implantation damage[9,10] but in the case of alloys of ZnO with TM has shown a tendency to form TM oxides precipitates.[8,11] Such new phases are very difficult to detect by means of x-ray diffraction, Raman, or high resolution electron microscopy due to the low amount of TM in the host sample. However, micro-x-ray absorption spectroscopy (μXAS) technique is an useful tool to elucidate the local coordination of these elements.

II. EXPERIMENT

Small pieces of ZnO (wurtzite) single crystal (MTI Crystal Corp.) with polished m-plane surface orientation and a nominal density of 5.2 g cm^{-3} were used as substrates. The implantation process was performed at normal incidence with 35 keV Mn^+ ions, with a total fluency of 4.2×10^{16} ions/cm^2 and an average current density of 0.4 μA cm^{-2}. Simulations of implantation profiles were carried out by the SRIM2006 code,[12] suggesting a Gaussian distribution with a maximum concentration peak at 20 nm from the surface and a straggling of 10 nm. After ion implantation these so-called continuum implanted samples were treated applying a rapid thermal annealing process in O_2 atmosphere at 800 °C for 3 min. μXAS and scanning x-ray fluorescence (XRF) measurements were carried out at the microprobe station ID22[3,13] of the European Synchrotron Radiation Facility. The beamline is equipped with two insertion devices, a flat Si mirror at 0.14° incident angle for harmonic rejection and a fixed-exit double Si(111) crystal monochromator ($\Delta E/E \sim 10^{-4}$). The monochromatic beam is focused on the sample down to a spot of 1.5×3.5 μm^2 size with a focus depth of 300 μm by means of a pair of mirrors in Kirkpatrick–Baez geometry. The intensity of the incident x-ray beam ($\sim 10^{11}$ photon/s in the focused beam at Mn K-edge) was monitored with an ionization chamber, while a Si drift detector was used to collect the characteristic x-ray emission lines. In fluorescence detection mode, μXAS measurement conditions at the Mn-K edge included a photon energy range of 6500–6650 eV and an energy step of 0.5 eV, and integration times determined by the counting statistics. XRF measurements were carried out with an incident angle of $\theta = 45 \pm 5°$ with respect to the sample surface to minimize the contribution of elastic scattering to the signal background. Micro-Raman spectra were recorded in Cry-

[a]Electronic mail: sanstres@esrf.fr.

 © 2010 American Institute of Physics

Downloaded 09 Feb 2010 to 161.111.180.191. Redistribution subject to AIP license or copyright; see http://jap.aip.org/jap/copyright.jsp

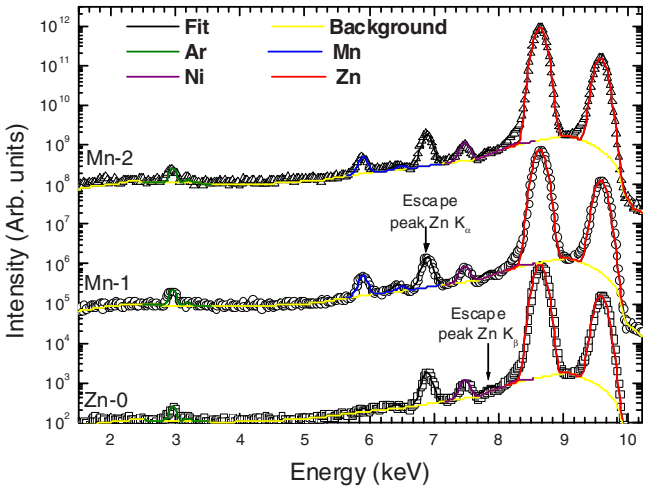

FIG. 1. (Color online) XRF spectra for ZnO single monocrystal (Zn-0), as-implanted ZnMnO (Mn-1), and thermal annealed implanted ZnMnO (Mn-2), shifted for clarity.

obench Facility of ESRF with a 514 nm excitation line of an Ar+ laser using a Renishaw Invia system[14] equipped with a compact probe compatible with an x-ray goniometer. The Raman scattering experiments were performed in back-scattering configuration with a spectral shift resolution better than 1 cm^{-1}.

III. RESULTS

In this work Zn-0, Mn-1, and Mn-2 labels correspond to ZnO single crystal, Mn implanted ZnO, and thermal annealed Mn implanted ZnO, respectively. The homogeneity of the Mn implantation was validated by measuring its fluorescence line intensity over 50×50 μm^2 sample area (not shown), taking advantage of the piezoelectric[1] scanning at the microprobe ID22. XRF measurements for Zn-0, Mn-1, and Mn-2 are shown in Fig. 1 on logarithmic scale (vertically shifted for clarity). "Escape peaks" have been observed in these spectra, generated from the Si drift detector as the combination of a Si K shell transition with the most intense peaks (in this case the Zn K energy peaks). The 12 keV excitation energy allows to measure the K shell lines of Zn, Mn, Ni, and Ar. The Ni traces are associated with the Zn-0 template and used as substrate for the implantation, and Ar line is originated from air. The implanted Mn concentration was calculated from the Mn and Zn shell line intensity ratio using PYMCA code,[15] giving around 0.2% of Mn in Mn-1 and Mn-2 samples. Within the detection limits of the technique, no traces of other elements were observed after implantation in the considered energy range. Thermal instability in oxidizing conditions is a crucial issue in future potential applications. It has already been reported in alloys or doped ZnO, such as ZnO:Ga (Ref. 16) or ZnFeO.[11]

Raman spectroscopy is a powerful tool to measure the characteristic vibration modes of the lattice and symmetry dependent phonon modes. Since ZnO crystallizes in the wurtzite structure belonging to the $C46v$ ($P63mc$) space group, the zone center phonons are 2A1+2B1+2E1+2E2, from which one A1, one E1, and two E2 are Raman active, whereas the B1 modes are silent. In addition, one set of A1

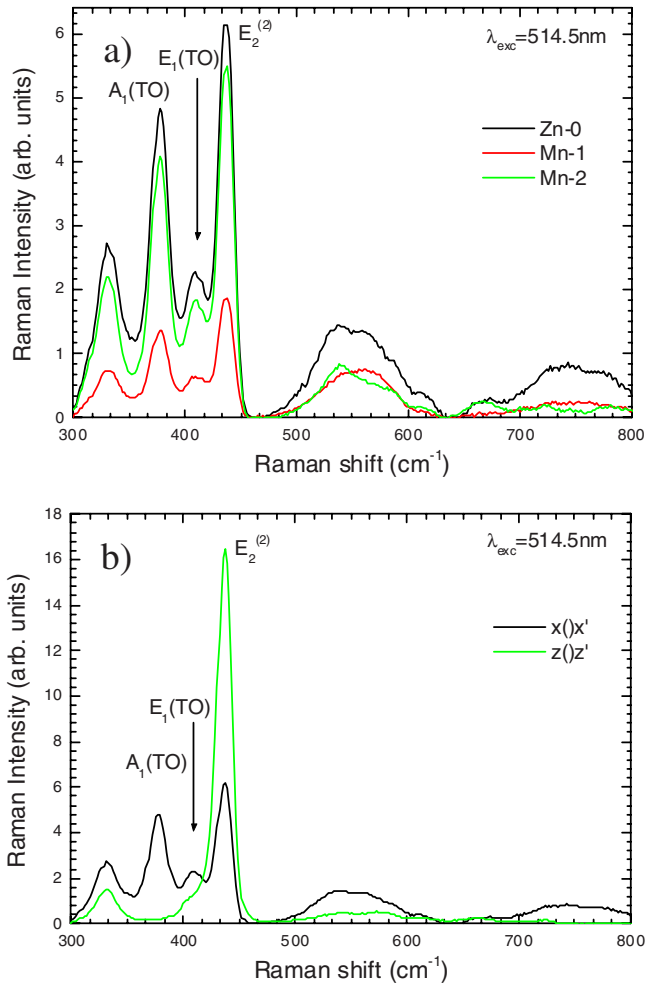

FIG. 2. (Color online) (a) Raman scattering spectra for samples Zn-0, Mn-1, and Mn-2. (b) Spectra of sample of Mn-1 for two configurations indicated in the figure.

and E1 corresponds to acoustic phonons. The anisotropic short-range order of the hexagonal structure is responsible for the A1-E1 splitting, whereas the long-range Coulomb field causes the polar modes split into longitudinal-transverse optical modes at the zone center. Figure 2 shows the Raman spectra for different configurations and samples. The findings indicate that the implanted elements are in substitutional site due to the absence of peaks related to other phases.[9] No differences between Zn-0, Mn-1, and Mn-2 spectra have been observed. Peaks located at 377, 410, and 437 cm^{-1} are assigned to ZnO A1(TO), E1(TO), and E2(2) Raman peaks respectively[17] and its appearance in spectra is determined by the selection rules of the wurtzite structure.[18] The second order Raman peak measured at 332 cm^{-1} has been associated in the literature[19] to the sum of two phonons coming from K-M-Σ transition at 160 cm^{-1}. Two major bands centered at 550 and 750 cm^{-1} with large bandwidths also correspond to overtones due to Fröhlich electron-phonon scattering. The effect of thermal annealing does not show any additional Raman peaks from secondary phases or disorder activated phonon modes. The presences of the peaks related to the Fröhlich electron-phonon scattering would hide the possible appearance of the characteristic Raman peak[20] of Mn_2O_3, which is located at 680 cm^{-1}.

Downloaded 09 Feb 2010 to 161.111.180.191. Redistribution subject to AIP license or copyright; see http://jap.aip.org/jap/copyright.jsp

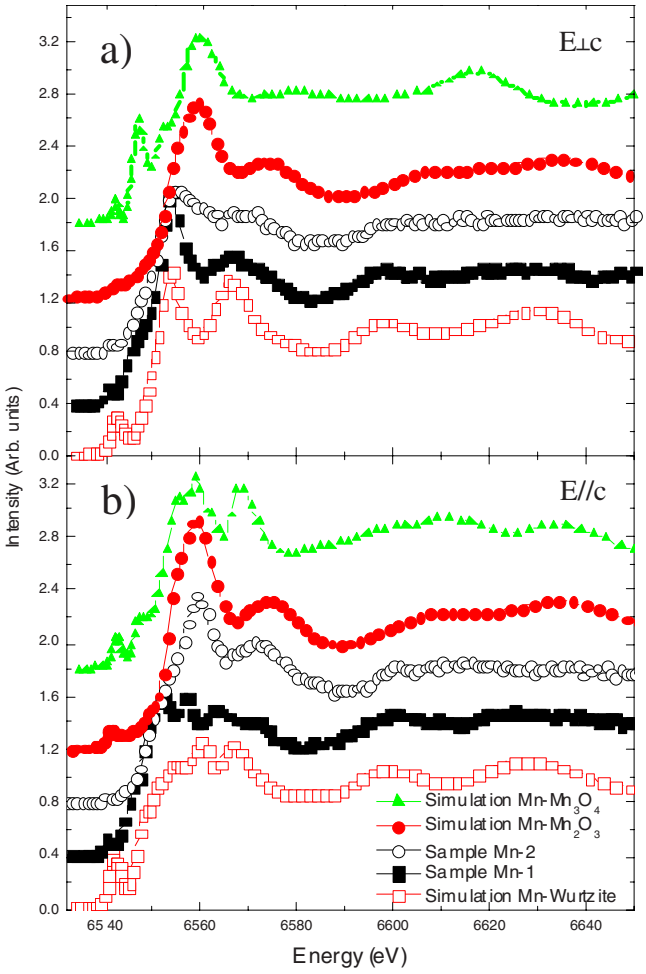

FIG. 3. (Color online) XANES data for samples Mn-1 and Mn-2. The figure also includes the theoretical simulations for Mn in substitutional site in ZnO and Mn in α-Mn_2O_3 structure: (a) with electric field perpendicular to the c-axis and (b) with electric field parallel to c-axis.

Linear polarization dependence of the x-ray absorption near edge structure (XANES) spectra gives a measurement of preferential directions and anisotropies in the local coordination of an element into a lattice. Figure 3 shows the study of the variation in XANES spectra around Mn K-edge with the electrical field vector parallel and perpendicular to the c-axis of the ZnO. The simulations performed at the Mn K edge using the *ab initio* self-consistent FEFF8 code[21] are also included in the figure for comparison. In our case, the anisotropy[22,23] of the wurtzite structure was also used to identify the influence of impurities into the local environment. Figure 3 displays the results obtained for sample Mn-1. The good agreement between the experimental Mn K-edge absorption spectrum and the simulation of Mn in substitutional Zn sites of ZnO shows that most of Mn cations are tetrahedrally coordinated by oxygen in sample Mn-1. Another indication of this fact is the strong resemblance between the Mn and Zn K-edges (not shown here). Small amounts of other phases cannot be completely neglected according to the sensitivity of this technique. For the parallel geometry (E∥c), for instance, apart from the most intense peaks located above the edge, the XANES spectrum of the as-implanted sample could look like to the one of Mn_3O_4 in the pre-edge and edge regions. However, the relative intensity of the different resonances, energy positions, as well as their polarization dependencies do not follow the same trend. The implication of Mn_3O_4 for such configuration (E∥c) was excluded based on linear combination analysis. Using the theoretical simulations of Mn with wurtzite and Mn_3O_4 coordinations, the resulting spectral shapes exhibit predominantly the dominant features at 6600 and 6626 eV coming from the characteristic Mn cations in tetrahedral sites (wurtzite), with an unclear and unconvincing role played by the Mn_3O_4. As a result, the observations around the white line could be due to the damage produced in the implantation, which would produce slight changes in the lineshape of the spectrum, namely, structural disorder around the Mn ion and/or a modification of the p-electronic density caused by defects[24] (vacancies, interstitial ions, etc.). The slight difference observed of the lineshape around the white line could be explained taking into account the damage produced in the implantation. This effect has already been studied for other implanted samples like cubic-BN,[25] where a change around the white line was observed with the variation in the kinetic energy of the implanted ions.

Figure 3 also displays the XANES spectra for sample Mn-2. The net difference between the experimental XANES spectra observed for the as-implanted sample and the annealed one could be considered as a fingerprint of a phase transition of a large amount of the Mn atoms. This change in the local coordination of Mn cations is related to the application of a thermal annealing in O_2 atmosphere. An oxygen-rich atmosphere in the thermal annealing would produce the formation of oxygen-richer structures such as spinels or certain Mn oxide phases. A comparison between the experimental data and several theoretical simulations was carried out in order to determine the crystalline structure formed (Mn_3O_4, Mn_2O_3, etc.). The results show that the change observed in the absorption spectrum of Mn K-edge in sample Mn-2 corresponds to the formation of α-Mn_2O_3 phase. Accordingly, the oxidation number of Mn shifts from +2 to +3 in a cubic bixbyite crystalline structure, where Mn would be octohedrally coordinated by oxygen. The diffusion of Zn into this phase was proposed[26] as a possible explanation for the origin of the ferromagnetism at room temperature observed in the literature. Nevertheless, the broad peaks located at 6600 and 6626 eV are characteristic features of wurtzite structure, which would indicate that a certain proportion of Mn atoms remain in substitutional position after the thermal annealing. Our finding is an interesting result, taking into account that the coexistence of ions with different oxidation number Mn^{2+} and Mn^{3+} has been proposed to play an important role in the ferromagnetism observed in GaMnN.[27] Some studies have extended this model to other wide band-gap TM alloys,[27] such as ZnMnO.

Figure 4(a) displays the x-ray Linear dichroism (XLD) signal for as-implanted sample (Mn-1), where the experimental spectrum fits to the theoretical simulation for Mn in wurtzite structure. As a matter of fact, this result supports the substitutional character of Mn into the ZnO host lattice. The XLD signal for the thermal annealed sample in oxidizing conditions (Mn-2) is shown in Fig. 4(b). The experimental

Downloaded 09 Feb 2010 to 161.111.180.191. Redistribution subject to AIP license or copyright; see http://jap.aip.org/jap/copyright.jsp

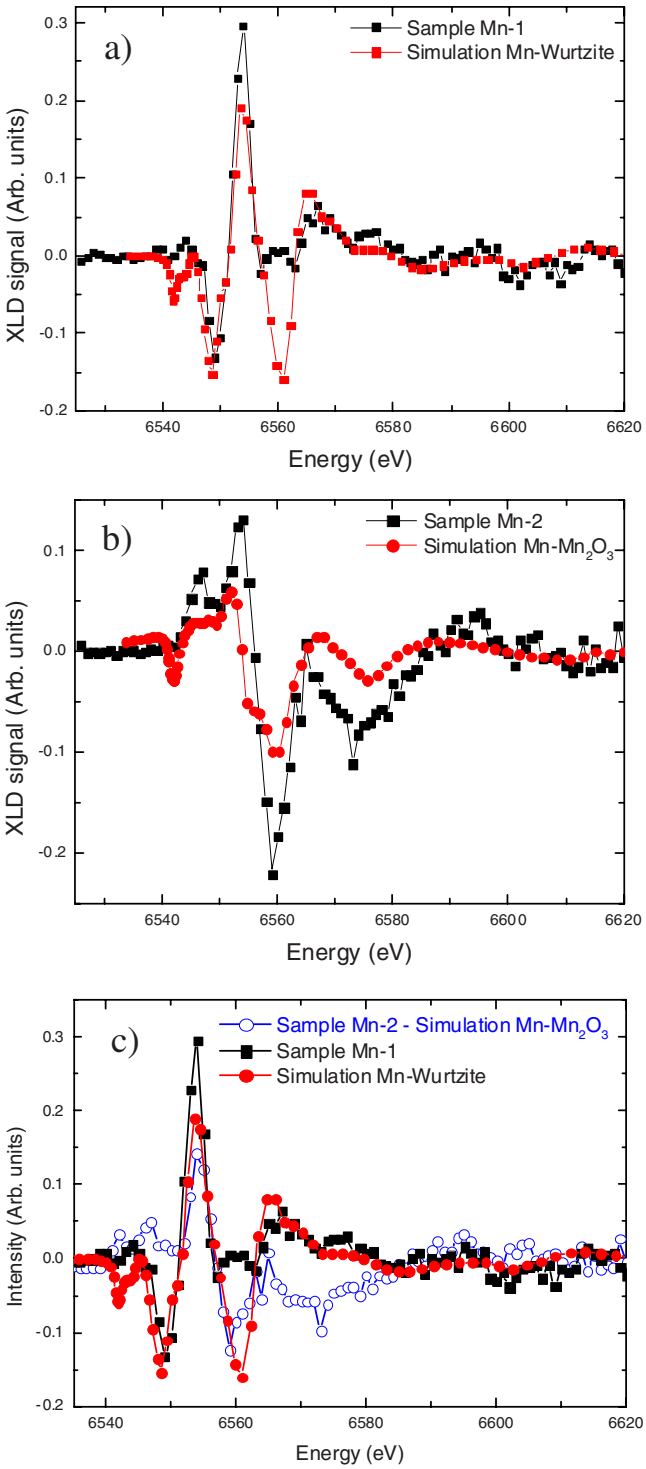

FIG. 4. (Color online) XLD signal obtained from (a) sample Mn-1 and theoretical simulation of Mn in wurtzite structure, (b) sample Mn-2 and theoretical simulation of Mn in α-Mn_2O_3 phase, and (c) subtraction between the theoretical simulation of Mn_2O_3 and the signal corresponding to the sample Mn-2 compared with XLD signal from Mn-1 sample. The simulation signal of Mn in wurtzite structure has been also included for comparison.

data present a similar spectral shape compared with the theoretical simulation for Mn in α-Mn_2O_3 phase. Nevertheless, a shoulder appears in the main peak, which would reveal the presence of Mn cations in a different crystalline structure. To explain this phenomenon, the theoretical XLD signal for Mn forming Mn_2O_3 was subtracted to the experimental one of the sample Mn-2 in order to distinguish the contribution of each different phase. A similar analysis was not doable for the unannealed sample because of the poor signal-to-noise ratio of the corresponding difference spectrum. In the annealed case, the resulting curve was compared to the experimental XLD signal obtained for sample Mn-1 [Fig. 4(c)]. The energy position of the dominant peak is equivalent for both signals (6554 eV). Regardless the signal amplitude, the correspondence could indicate that a certain amount of Mn cations remains in wurtzite structure even after the thermal annealing in oxidizing conditions, coherently with the assumptions done in the analysis of the polarization dependent XANES spectra. The ratio between the intensities of the main peak would allow to determine roughly the relative proportion of Mn cations remaining in substitutional site into ZnO host lattice respect to the implanted sample. Our calculation works out that ~50% of Mn remains in wurtzite structure after the thermal annealing.

IV. CONCLUSIONS

In summary, the structural properties of Mn implanted ZnO samples and its thermal stability was investigated by a multimodal analysis using x-ray microspectroscopic techniques. XRF measurements showed no traces of contamination during the growth process. Raman spectra exhibited the unambiguous signature of the ZnO wurtzite structure without secondary phases even after the thermal annealing. XANES and XLD measurements revealed Mn ions in substitutional sites in the ZnO host lattice for as-implanted sample. A phase transition is produced in a large amount of Mn atoms after the thermal annealing in oxidizing conditions. Moreover, the coexistence of Mn in wurtzite structure and Mn in a new crystalline structure was presented and tentatively attributed to the segregation of Mn in α-Mn_2O_3 phase.

ACKNOWLEDGMENTS

The authors thank to Dr. G. Gonzalez for providing the implantation system and Professor M. Vazquez for financial support.

[1]T. Dietl, H. Ohono, F. Matsukura, J. Cibert, and D. Ferrand, Science **287**, 1019 (2000).
[2]G. Martinez-Criado, A. Segura, J. A. Sans, A. Homs, J. Pellicer-Porres, and J. Susini, Appl. Phys. Lett. **89**, 061906 (2006).
[3]J. M. D. Coey, M. Venkatesan, and C. B. Fitzgerald, Nature Mater. **4**, 173 (2005).
[4]J. H. Park, M. G. Kim, H. M. Jang, S. Ryu, and Y. M. Kim, Appl. Phys. Lett. **84**, 1338 (2004).
[5]S. Kolesnik, B. Dabrowski, and J. Mais, J. Appl. Phys. **95**, 2582 (2004).
[6]D. P. Norton, M. E. Overberg, S. J. Pearton, K. Pressner, J. D. Budai, L. A. Boatner, M. F. Chisholm, J. S. Lee, Z. G. Khim, Y. D. Park, and R. G. Wilson, Appl. Phys. Lett. **83**, 5488 (2003).
[7]T. Dietl, T. Andrearczyk, A. Lipinska, M. Kiecana, M. Tay, and Y. Wu, Phys. Rev. B **76**, 155312 (2007).
[8]S. Zhou, K. Potzger, G. Talut, H. Reuther, J. von Borany, R. Grotzschel, W. Skorupa, M. Helm, and J. Fassbender, J. Appl. Phys. **103**, 023902 (2008).
[9]M. Schumm, M. Koerdel, S. Muller, H. Zutz, C. Ronning, J. Stehr, D. M. Hofmann, and J. Geurts, New J. Phys. **10**, 043004 (2008).
[10]S. Ramachandran, J. Narayan, and J. T. Prater, Appl. Phys. Lett. **88**, 242503 (2006).
[11]S. Zhou, K. Potzger, J. von Borany, R. Grotzschel, W. Skorupa, M. Helm, and J. Fassbender, Phys. Rev. B **77**, 035209 (2008).
[12]www.srim.org.

Downloaded 09 Feb 2010 to 161.111.180.191. Redistribution subject to AIP license or copyright; see http://jap.aip.org/jap/copyright.jsp

[13]G. Martinez-Criado, A. Somogyi, S. Ramos, J. Campo, R. Tucoulou, M. Salome, J. Susini, M. Hermann, M. Eickhoff, and M. Stutzmann, Appl. Phys. Lett. **86**, 131927 (2005).
[14]P. Carpentier, A. Royant, J. Ohana, and D. Bourgeois, J. Appl. Crystallogr. **40**, 1113 (2007).
[15]V. A. Solé, E. Papillon, M. Cotte, Ph. Walter, and J. Susini, Spectrochim. Acta, Part B **62**, 63 (2007).
[16]J. A. Sans, G. Martinez-Criado, J. Pellicer-Porres, J. F. Sanchez-Royo, and A. Segura, Appl. Phys. Lett. **91**, 221904 (2007).
[17]F. Decremps, J. Pellicer-Porres, A. Marco Saitta, J.-C. Chervin, and A. Polian, Phys. Rev. B **65**, 092101 (2002).
[18]P. Dahan, V. Fleurov, and K. Kikoin, J. Phys.: Condens. Matter **9**, 5355 (1997).
[19]J. M. Calleja and M. Cardona, Phys. Rev. B **16**, 3753 (1977).
[20]F. Buciuman, F. Patcas, R. Craciun, and D. R. T. Zahn, Phys. Chem. Chem. Phys. **1**, 185 (1999).
[21]A. L. Ankudinov, B. Ravel, J. J. Rehr, and S. D. Conradson, Phys. Rev. B **58**, 7565 (1998).
[22]G. Martínez-Criado, O. Sancho-Juan, N. Garro, J. A. Sans, A. Cantarero, J. Susini, M. Roever, D.-D. Mai, A. Bedoya-Pinto, J. Malindretos, and A. Rizzi, Appl. Phys. Lett. **93**, 021916 (2008).
[23]F. J. Manjon, D. Errandonea, A. H. Romero, N. Garro, J. Serrano, and M. Kuball, Phys. Rev. B **77**, 205204 (2008).
[24]C. Mignote, Nucl. Instrum. Methods Phys. Res. B **187**, 95 (2002).
[25]R. Gago, B. Abendroth, J. I. Cerda, I. Jimenez, and W. Moller, Phys. Rev. B **76**, 174111 (2007).
[26]D. C. Kundaliya, S. B. Ogale, S. E. Lofland, S. Dhar, C. J. Metting, S. R. Shinde, Z. Ma, B. Varughese, K. V. Ramanujachary, L. Salamanca-Riba, and T. Venkatesan, Nature Mater. **3**, 709 (2004).
[27]S. Sonoda, I. Tanaka, H. Ikeno, T. Yamamoto, F. Oba, T. Araki, Y. Yamamoto, K. Suga, Y. Nanishi, Y. Akasaka, K. Kindo, and H. Hori, J. Phys.: Condens. Matter **18**, 4615 (2006).

Downloaded 09 Feb 2010 to 161.111.180.191. Redistribution subject to AIP license or copyright; see http://jap.aip.org/jap/copyright.jsp